Journal of
Mechanics of
Materials and Structures

ELECTROMECHANICAL FIELDS IN A NONUNIFORM PIEZOELECTRIC SEMICONDUCTOR ROD

Guangying Yang, Jianke Du, Ji Wang and Jiashi Yang

Volume 13, No. 1 January 2018

msp

JOURNAL OF MECHANICS OF MATERIALS AND STRUCTURES
Vol. 13, No. 1, 2018
dx.doi.org/10.2140/jomms.2018.13.103

ELECTROMECHANICAL FIELDS IN A NONUNIFORM PIEZOELECTRIC SEMICONDUCTOR ROD

GUANGYING YANG, JIANKE DU, JI WANG AND JIASHI YANG

We study electromechanical fields in a piezoelectric semiconductor rod nonuniformly doped with impurities producing holes and electrons. The phenomenological theory of piezoelectric semiconductors consisting of the equations of piezoelectricity and the conservation of charge for holes and electrons is used, which was reduced to a one-dimensional model for thin rods in a previous paper. In this paper the one-dimensional theory is linearized for low electric potential or voltage. Solutions from the linearized one-dimensional equations are obtained for three specific doping profiles: linear doping, piecewise linear doping with fundamentally important applications in PN junctions, and sinusoidal doping. Various electromechanical fields produced by the doping are calculated and examined. The results are fundamental to piezoelectric semiconductor devices or piezotronics.

1. Introduction

Piezoelectric materials can be dielectrics (insulators) or semiconductors although most of the time they are used as dielectrics. Historically, there were early attempts on making piezoelectric semiconductor devices decades ago but the research essentially became dormant (see the review [Hickernell 2003]). However, relatively recently, various piezoelectric semiconductor nanostructures have been synthesized such as ZnO fibers, tubes, belts, spirals and films [Wang 2003; 2010; Kumar and Kim 2011; Lee et al. 2012; 2014]. They can be made into single structures [Gao and Wang 2009; Hu et al. 2010; Araneo et al. 2012; Ji et al. 2013] or in arrays [Shen et al. 2010; Chen et al. 2007; Yoo et al. 2009; Xue et al. 2010], and have been used to make energy harvesters for converting mechanical energy into electrical energy [Gao et al. 2007; Choi et al. 2009; Romano et al. 2011; Asthana et al. 2014; Liao et al. 2014], field effect transistors [Wang 2003; 2010; Wang et al. 2006], acoustic charge transport devices [Büyükköse et al. 2014], as well as strain, gas, humidity and chemical sensors [Wang 2003; Yu et al. 2010]. The study of piezoelectric semiconductor materials and devices is growing rapidly and has formed a new research area called piezotronics. It also presents a new class of coupled-field problems in mechanics.

For device application, the basic behaviors of piezoelectric semiconductors regarding the motion of charge carriers under the action of the electric potential produced by mechanical loads through piezoelectric coupling can be described by a phenomenological theory [Hutson and White 1962] consisting of the equations of linear piezoelectricity [Auld 1973] and the conservation of charge for electrons and holes [Pierret 1983]. Because of the anisotropy of piezoelectric materials, the electromechanical couplings in them, and the nonlinearity associated with the drift currents of electrons and holes which are the products of the unknown carrier concentrations and the unknown electric field [Pierret 1983], theoretical analyses of piezoelectric semiconductor devices normally present considerable mathematical challenges. In spite

Keywords: piezoelectric, semiconductor, piezotronics.

of the mathematical difficulties, researchers have studied a series of useful problems of piezoelectric semiconductors including thickness vibration of plates [Wauer and Suherman 1997; Li et al. 2015], propagation of plate and surface waves [Collet 2008; Gu and Jin 2015], electromechanical fields around a hole [Zhang and Hu 2014] and in an inclusion [Yang et al. 2006], fields near cracks [Yang 2005; Hu et al. 2007; Sladek et al. 2014a; 2014b; Zhao et al. 2016a; 2016b; Fan et al. 2016], fields and waves in a rod with excessive electrons [Zhang et al. 2016a; 2016b], static extension of a fiber [Zhang et al. 2017a; 2017b], static bending of a fiber [Gao and Wang 2007; 2009; Fan et al. 2017; Zhang et al. $\geq$ 2018], and structural theories of plates [Yang and Zhou 2005], shells [Yang et al. 2005], and rods [Li et al. $\geq$ 2018].

In this paper we study electromechanical fields in a nonuniformly doped piezoelectric semiconductor rod. We consider three specific doping profiles. The case of linear doping is for the most basic understanding of nonuniform doping. The case of piecewise linear doping is for the understanding of the formation of a PN junction and the prediction of its structure and fields, which is fundamentally important in piezotronics applications. The case of sinusoidal doping is for some further understanding of nonuniform doping with potentials in applications.

2. Phenomenological theory of piezoelectric semiconductors

This section presents a brief summary of the three-dimensional theory of piezoelectric semiconductors. We use the Cartesian tensor notation. The indices i, j, k, and l assume 1, 2, and 3. A comma followed by an index indicates a partial derivative with respect to the coordinate associated with the index. A superimposed dot represents a time derivative. The theory consists of [Auld 1973; Pierret 1983]

$$T_{ji,j} = \rho\ddot{u}_i, \quad D_{i,i} = \rho^e = q(p - n + N_D^+ - N_A^-), \quad J_{i,i}^p = -q\dot{p}, \quad J_{i,i}^n = q\dot{n}, \tag{1}$$

where $\boldsymbol{T}$ is the stress tensor, ρ the mass density, $\boldsymbol{u}$ the mechanical displacement vector, $\boldsymbol{D}$ the electric displacement vector, ρ^e the charge density, $q = 1.6 \times 10^{-19}$ C the electronic charge, p and n the concentrations of holes and electrons, N_D^+ and N_A^- the concentrations of impurities of donors and accepters, and J_i^p and J_i^n the hole and electron current densities. Equation $(1)_1$ is the stress equation of motion or the linear momentum equation (Newton's law). Equation $(1)_2$ is the charge equation of electrostatics (Gauss's law). Equations $(1)_3$ and $(1)_4$ are the conservation of charge for electrons and holes, respectively which are also called continuity equations. Constitutive relations accompanying (1) can be written in the form [Auld 1973; Pierret 1983]

$$\begin{aligned} \boldsymbol{S}_{ij} &= s_{ijkl}^{\boldsymbol{E}} T_{kl} + d_{kij} E_k, & D_i &= d_{ikl} T_{kl} + \varepsilon_{ik}^T E_k, \\ J_i^p &= qp\mu_{ij}^p E_j - qD_{ij}^p p_{,j}, & J_i^n &= qn\mu_{ij}^n E_j + qD_{ij}^n n_{,j}, \end{aligned} \tag{2}$$

where $\boldsymbol{S}$ is the strain tensor, $\boldsymbol{E}$ the electric field vector, s_{ijkl}^E the elastic compliance, d_{kij} the piezoelectric constants, ε_{ij}^T the dielectric constants, μ_{ij}^n and μ_{ij}^p the carrier mobility, D_{ij}^n and D_{ij}^p the carrier diffusion constants. The equations on the first line of (2) are the usual constitutive relations for piezoelectric materials. Those on the second line are for hole and electron currents including both drift currents under an electric field and diffusion currents due to concentration gradients. The strain $\boldsymbol{S}$ and the electric field $\boldsymbol{E}$ are related to the mechanical displacement $\boldsymbol{u}$ and the electric potential φ through

$$S_{ij} = \tfrac{1}{2}(u_{i,j} + u_{j,i}), \quad E_i = -\varphi_{,i}. \tag{3}$$

3. One-dimensional equations for the extension of a rod

Consider the piezoelectric semiconductor rod shown in Figure 1. The shape of the cross section A of the rod may be arbitrary. The rod is assumed to be long and thin, i.e., its length is much larger than the characteristic dimension of the cross section. It is made from a piezoelectric semiconductor crystal of class 6 mm. The c-axis of the crystal is along the axis of the rod. The lateral surface of the rod is free. The electric field in the surrounding free space is neglected.

We are interested in the extensional deformation of the rod which can be described by a set of one-dimensional equations for the axial displacement u_3 and the axial stress $T_3 = T_{33}$. In the one-dimensional model, (1) reduces to [Zhang et al. 2017a]

$$\begin{aligned} &\frac{\partial T_3}{\partial x_3} = \rho \ddot{u}_3, \qquad \frac{\partial D_3}{\partial x_3} = \rho^e = q(p - n + N_D^+ - N_A^-), \\ &q\dot{p} = -\frac{\partial J_3^p}{\partial x_3}, \qquad q\dot{n} = \frac{\partial J_3^n}{\partial x_3}. \end{aligned} \tag{4}$$

The relevant one-dimensional constitutive relations are [Zhang et al. 2017a]

$$\begin{aligned} &T_3 = \bar{c}_{33} S_3 - \bar{e}_{33} E_3, \qquad D_3 = \bar{e}_{33} S_3 + \bar{\varepsilon}_{33} E_3, \\ &J_3^p = qp\mu_{33}^p E_3 - qD_{33}^p \frac{\partial p}{\partial x_3}, \quad J_3^n = qn\mu_{33}^n E_3 + qD_{33}^n \frac{\partial n}{\partial x_3}. \end{aligned} \tag{5}$$

Here, $\bar{c}_{33}$, $\bar{e}_{33}$, and $\bar{\varepsilon}_{33}$ are the effective one-dimensional elastic, piezoelectric, and dielectric constants. They are related to the usual three-dimensional material constants s_{pq}^E, ε_{ij}^T and d_{ip} through

$$\bar{c}_{33} = 1/s_{33}^E, \quad \bar{e}_{33} = d_{33}/s_{33}^E, \quad \bar{\varepsilon}_{33} = \varepsilon_{33}^T - d_{33}^2/s_{33}^E. \tag{6}$$

The appearance of the effective one-dimensional material constants in (5) is because of the introduction of the one-dimensional stress relaxation condition that for thin rods we approximately have $T_1 = T_2 = 0$. The mobility and diffusion constants in (5), μ_{33}^p, μ_{33}^n, D_{33}^p, and D_{33}^n, satisfy the Einstein relation

$$\frac{\mu_{33}^p}{D_{33}^p} = \frac{\mu_{33}^n}{D_{33}^n} = \frac{q}{k_B T}, \tag{7}$$

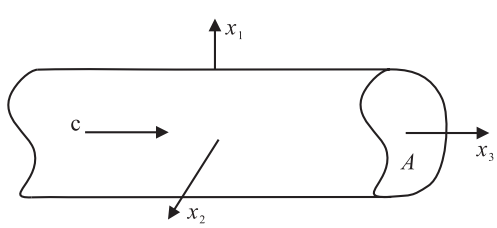

Figure 1. A piezoelectric semiconductor rod of crystals of class 6 mm.

where k_B is the Boltzmann constant and T the absolute temperature. The relevant strain-displacement relation and the electric field-potential relation are

$$S_3 = \frac{\partial u_3}{\partial x_3}, \quad E_3 = -\frac{\partial \varphi}{\partial x_3}. \tag{8}$$

4. Static fields in a rod

Consider a rod in equilibrium. From $(4)_1$,

$$T_3 = C_1, \tag{9}$$

where C_1 is an integration constant. From $(5)_1$,

$$S_3 = \frac{1}{\bar{c}_{33}}(C_1 + \bar{e}_{33}E_3). \tag{10}$$

Substituting (10) and $(8)_2$ into $(5)_2$, we obtain

$$D_3 = \frac{\bar{e}_{33}}{\bar{c}_{33}}C_1 + \left(\bar{\varepsilon}_{33} + \frac{\bar{e}_{33}^2}{\bar{c}_{33}}\right)E_3 = \frac{\bar{e}_{33}}{\bar{c}_{33}}C_1 - \varepsilon_{33}\varphi_{,3}. \tag{11}$$

From $(4)_{3,4}$, J_3^p and J_3^n are constants. When the rod is electrically isolated at its two ends without currents, which we assume to be the case in this paper, these constants are zero. From $(5)_{3,4}$ and $(8)_2$,

$$J_3^p = -qp\mu_{33}^p\frac{\partial \varphi}{\partial x_3} - qD_{33}^p\frac{\partial p}{\partial x_3} = 0, \quad J_3^n = -qn\mu_{33}^n\frac{\partial \varphi}{\partial x_3} + qD_{33}^n\frac{\partial n}{\partial x_3} = 0. \tag{12}$$

With the use of (7), we rewrite (12) as

$$\frac{1}{p}\frac{\partial p}{\partial x_3} = -\frac{q}{k_BT}\frac{\partial \varphi}{\partial x_3}, \quad \frac{1}{n}\frac{\partial n}{\partial x_3} = \frac{q}{k_BT}\frac{\partial \varphi}{\partial x_3}. \tag{13}$$

Equation (13) can be integrated to produce

$$p = p_0\exp\left(-\frac{q}{k_BT}\varphi\right), \quad n = n_0\exp\left(\frac{q}{k_BT}\varphi\right), \tag{14}$$

where p_0 and n_0 are integration constants. Physically they are the values of p and n at $\varphi = 0$. The substitution of (11) and (14) into $(4)_2$ gives the following single equation governing the electric potential:

$$-\varepsilon_{33}\varphi_{,33} = q\left[p_0\exp\left(-\frac{q}{k_BT}\varphi\right) - n_0\exp\left(\frac{q}{k_BT}\varphi\right) + N_D^+(x_3) - N_A^-(x_3)\right]. \tag{15}$$

For small φ, we make the following approximation (14):

$$p \cong p_0\left(1 - \frac{q}{k_BT}\varphi\right), \quad n \cong n_0\left(1 + \frac{q}{k_BT}\varphi\right), \tag{16}$$

which can describe small carrier concentration variations. Substituting (16) into (15), we obtain a linear equation for the potential:

$$\varphi_{,33} = -\frac{q}{\varepsilon_{33}}\left[p_0 - n_0 - (p_0 + n_0)\frac{q}{k_BT}\varphi + N_D^+(x_3) - N_A^-(x_3)\right], \tag{17}$$

which can be further written as

$$\varphi_{,33} - \kappa^2 \varphi = -\frac{q}{\varepsilon_{33}}\left[p_0 - n_0 + N_D^+(x_3) - N_A^-(x_3)\right], \tag{18}$$

where

$$\kappa^2 = \frac{q}{\varepsilon_{33}}(p_0 + n_0)\frac{q}{k_B T}. \tag{19}$$

The general solution to (18) can be written as

$$\varphi = C_2 \sinh \kappa(x_3 + L) + C_3 \sinh \kappa(x_3 - L) + \frac{q}{\kappa^2 \varepsilon_{33}}(p_0 - n_0) + \varphi^p(x_3), \tag{20}$$

where C_2 and C_3 are integration constants, and φ^p is a particular solution of the nonhomogeneous equation

$$\varphi^p_{,33} - \kappa^2 \varphi^p = -\frac{q}{\varepsilon_{33}}[N_D^+(x_3) - N_A^-(x_3)]. \tag{21}$$

Once φ is known, p and n can be obtained from (16). With φ known, for the mechanical displacement, from (10), we have

$$u_{3,3} = \frac{1}{\bar{c}_{33}}(C_1 - \bar{e}_{33}\varphi_{,3}). \tag{22}$$

Integrating (22), we obtain

$$u_3 = \frac{1}{\bar{c}_{33}}(C_1 x_3 - \bar{e}_{33}\varphi) + C_4, \tag{23}$$

where C_4 is an integration constant.

We consider a free rod with the following boundary conditions:

$$T_{33}(\pm L) = 0, \quad J_3^p(\pm L) = 0, \quad J_3^n(\pm L) = 0, \quad D_3(\pm L) = 0. \tag{24}$$

When $C_1 = 0$, $(24)_1$ is satisfied. The satisfaction of $(24)_{2,3}$ is ensured by (12). Only $(24)_4$ remains which, according to (11), translates into

$$\varphi_{,3}(\pm L) = 0. \tag{25}$$

From (20), it can be seen that (25) determines C_2 and C_3 formally in terms of p_0 and n_0. Then (24) is completely satisfied. We need additional conditions to determine the remaining integration constants C_4, p_0, and n_0. Since (4), (5), (8), and (24) are invariant under a rigid-body translation of the rod in the x_3 direction, to fix the rigid-body displacement so that the displacement is unique, we choose the center of the rod as a reference for the displacement and impose

$$u_3(0) = 0. \tag{26}$$

Equation (26) formally determines C_4. At this point, (24)–(26) are all satisfied, and C_1–C_4 are all formally determined. There are two undetermined constants left, i.e., p_0 and n_0. Similar to (26), we also choose the center of the rod as the reference of the electric potential and set

$$\varphi(0) = 0. \tag{27}$$

Equation (27) determines a relationship between p_0 and n_0. To completely determine p_0 and n_0, we specify the total holes in the rod by the global charge neutrality condition

$$\int_{-L}^{L} (p - N_A^-)\, \mathrm{d}x_3 = 0. \tag{28}$$

Since $(4)_2$ and $(24)_4$ imply that

$$\int_{-L}^{L} (p - n + N_D^+ - N_A^-)\, \mathrm{d}x_3 = 0, \tag{29}$$

(28) and (29) further imply that

$$\int_{-L}^{L} (-n + N_D^+)\, \mathrm{d}x_3 = 0. \tag{30}$$

Therefore (28) is the only independent charge neutrality condition. Equations (27) and (28) determine p_0 and n_0.

5. Uniform and linear doping

For some basic understanding of the effect of a nonuniform doping, we begin with the simple case of uniform and linear doping. Let

$$N_A^-(x_3) = b_1 x_3 + c_1, \quad N_D^+(x_3) = b_2 x_3 + c_2. \tag{31}$$

Hence,

$$N_D^+(x_3) - N_A^-(x_3) = b x_3 + c, \quad b = b_2 - b_1, \quad c = c_2 - c_1. \tag{32}$$

In this case a particular solution of (21) is simply

$$\varphi^p = \frac{q}{\varepsilon_{33}\kappa^2}(b x_3 + c). \tag{33}$$

Therefore, the effects of a uniform or linear doping on the electric potential and p as well as n according to (16) are also uniform and linear. We also notice that in this case (27) and (28) take the following forms:

$$(p_0 - n_0) + c = 0, \tag{34}$$

$$p_0 = \frac{3c_1 n_0}{6n_0 - 3c_2}. \tag{35}$$

In the special case of a linear doping only with $c_1 = c_2 = 0$, i.e., without the uniform doping term, we have $p_0 = n_0 = 0$.

6. Piecewise linear doping and PN junction

PN junctions are the fundamental building blocks of many piezoelectric semiconductor devices [Lee et al. 2012; 2014; Chung et al. 2012]. The understanding of PN junctions in these materials and the prediction of the electromechanical fields near a PN junction are fundamentally important to the development of piezoelectric semiconductor devices. PN junctions between two piezoelectric semiconductor half spaces and between a circular cylinder and its surrounding material were analyzed in [Luo et al. $\geq$ 2018a;

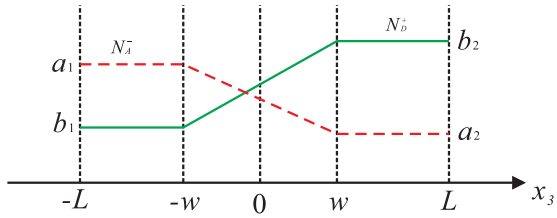

Figure 2. Piecewise linear doping.

≥ 2018b], respectively. In this section we show that PN junctions in a piezoelectric semiconductor rod can be produced by nonuniform doping. Consider the case when the left half of the rod is mainly p-doped and the right half mainly n-doped. Between the two halves there is a finite transition zone of width $2w$ in which the doping varies linearly as shown in Figure 2. Because of diffusion of the holes and electrons related to the doping, a PN junction may form in and near the transition zone. The PN junctions studied in [Luo et al. ≥ 2018a; ≥ 2018b] do not have a finite transition zone and effectively correspond to the special case of $w = 0$ in Figure 2, which is an ideal case simplified for theoretical analysis. In real applications usually there is a transition zone with a nonzero w.

Quantitatively, the doping profile in Figure 2 is described by

$$N_A^- = \begin{cases} a_1 & -L < x_3 < -w, \\ a_1 + \dfrac{a_2 - a_1}{2w}(x_3 + w) & |x_2| < w, \\ a_2 & w < x_3 < L, \end{cases} \tag{36}$$

and

$$N_D^+ = \begin{cases} b_1 & -L < x_3 < -w, \\ b_1 + \dfrac{b_2 - b_1}{2w}(x_3 + w) & |x_2| < w, \\ b_2 & w < x_3 < L. \end{cases} \tag{37}$$

Then,

$$N_D^+ - N_A^- = \begin{cases} d_1, & -L < x_3 < -w, \\ d_3 + d_4 x_3, & |x_3| < w, \\ d_2, & w < x_3 < L, \end{cases} \tag{38}$$

where

$$d_1 = b_1 - a_1, \quad d_2 = b_2 - a_2, \quad d_3 = \frac{b_1 - a_1}{2} + \frac{b_2 - a_2}{2}, \quad d_4 = \frac{b_2 - b_1}{2w} - \frac{a_2 - a_1}{2w}. \tag{39}$$

PN junctions are local. It is sufficient to consider the special and relatively simple case when $L = \infty$. In this case, from (21), (20), (16), and (23), we have, for $x_3 < -w$,

$$\begin{gathered} \varphi^p = \frac{q}{\varepsilon_{33}\kappa^2} d_1, \quad \varphi = C_1 \exp \kappa(x_3 + w) + \frac{q}{\kappa^2 \varepsilon_{33}}(p_0 - n_0) + \varphi^p(x_3), \\ p \cong p_0\Big(1 - \frac{q}{k_B T}\varphi\Big), \quad n \cong n_0\Big(1 + \frac{q}{k_B T}\varphi\Big), \quad u_3 = -\frac{\bar{e}_{33}}{\bar{c}_{33}}\varphi + C_2, \\ D_3 = -\varepsilon_{33}\varphi_{,3}, \quad T_3 = 0, \quad J_3^p = 0, \quad J_3^n = 0, \end{gathered} \tag{40}$$

and, similarly for $w < x_3$,

$$\begin{gathered}\varphi^p = \frac{q}{\varepsilon_{33}\kappa^2}d_2, \quad \varphi = C_3 \exp\kappa(w-x_3) + \frac{q}{\kappa^2\varepsilon_{33}}(p_0-n_0) + \varphi^p(x_3),\\ p \cong p_0\Big(1-\frac{q}{k_BT}\varphi\Big), \quad n \cong n_0\Big(1+\frac{q}{k_BT}\varphi\Big), \quad u_3 = -\frac{\bar{e}_{33}}{\bar{c}_{33}}\varphi + C_4,\\ D_3 = -\varepsilon_{33}\varphi_{,3}, \quad T_3 = 0, \quad J_3^p = 0, \quad J_3^n = 0.\end{gathered} \tag{41}$$

Equation (40) and (41) show that κ describes the exponentially decaying rate of the fields from the edges of the transition zone. Inside the transition zone where $|x_3| < w$, we have

$$\begin{gathered}\varphi^p = \frac{q}{\varepsilon_{33}\kappa^2}(d_3+d_4x_3), \quad \varphi = C_5\sinh\kappa(x_3+w)+C_6\sinh\kappa(x_3-w)+\frac{q}{\kappa^2\varepsilon_{33}}(p_0-n_0)+\varphi^p(x_3),\\ p \cong p_0\Big(1-\frac{q}{k_BT}\varphi\Big), \quad n \cong n_0\Big(1+\frac{q}{k_BT}\varphi\Big), \quad u_3 = -\frac{\bar{e}_{33}}{\bar{c}_{33}}\varphi+C_7,\\ D_3 = -\varepsilon_{33}\varphi_{,3}, \quad T_3 = 0, \quad J_3^p = 0, \quad J_3^n = 0.\end{gathered} \tag{42}$$

The boundary and continuity conditions are (24) when $L = \infty$, and

$$\begin{gathered}T_{33}(\pm w^-) = T_{33}(\pm w^+), \quad J_3^p(\pm w^-) = J_3^p(\pm w^+),\\ J_3^n(\pm w^-) = J_3^n(\pm w^+), \quad D_3(\pm w^-) = D_3(\pm w^+),\end{gathered} \tag{43}$$

as well as

$$\begin{gathered}u_3(\pm w^-) = u_3(\pm w^+), \quad \varphi(\pm w^-) = \varphi(\pm w^+),\\ p(\pm w^-) = p(\pm w^+), \quad n(\pm w^-) = n(\pm w^+).\end{gathered} \tag{44}$$

Equation (24) when $L = \infty$ and $(43)_{1\text{–}3}$ are already satisfied. Equation $(44)_2$ implies $(44)_{3,4}$. From $(43)_4$ and $(44)_{1,2}$, we have six conditions left. With (26)–(28) where $L = \infty$, there are nine equations for C_1–C_7, p_0, and n_0. They are solved on a computer.

As a numerical example, consider a ZnO rod whose material constants can be founded in [Auld 1973]:

$$\varepsilon_{33} = 12.64\varepsilon_0 = 1.119\times10^{-10}\,\mathrm{F/m}, \quad c_{33} = 21.09\times10^{10}\,\mathrm{N/m^2}, \quad e_{33} = 1.32\,\mathrm{C/m^2}, \tag{45}$$

where the dielectric constant of free space is $\varepsilon_0 = 8.8537\times10^{-12}\,\mathrm{F/m}$. At room temperature, we have [Pierret 1996]

$$\frac{\mu_{33}^n}{D_{33}^n} = \frac{\mu_{33}^p}{D_{33}^p} = \frac{q}{k_BT} = 38.46\,\mathrm{V^{-1}}. \tag{46}$$

We consider the following case with some symmetry or antisymmetry:

$$a_1 = b_2 = 1.0\times10^{21}\,\mathrm{m^{-3}}, \quad a_2 = b_1 = 0.8a_1, \quad w = 0.1\,\mu\mathrm{m}. \tag{47}$$

In this case, it is found that

$$p_0 = n_0 = 0.9\times10^{21}\,\mathrm{m^{-3}} = \tfrac{1}{2}(a_1+a_2) = \tfrac{1}{2}(b_1+b_2). \tag{48}$$

From (19),

$$\frac{1}{\kappa} = 1.005\times10^{-7} \cong 0.1\,\mu\mathrm{m}, \tag{49}$$

which is a characteristic length of the exponentially varying fields. Numerical results show that in this case,

$$\frac{q}{k_B T}\varphi \cong 0.1154. \tag{50}$$

Hence the linear approximation in (16) is valid.

Figure 3 shows the contour plots of various electromechanical fields inside and near the transition zone. The diameter d of the rod in the figure is symbolic only and is immaterial for a one-dimensional model. Figures 3a and 3b are the concentrations of holes and electrons which were initially determined by the piecewise linear functions in Figure 2 but are now smooth because of diffusion. They are monotonically changing along the rod, more rapidly in the transition zone. Figure 3c shows essentially the net or total charge which localizes within and near the transition zone, and has a sign change there (the formation of a PN junction). Figure 3d shows the local electric field produced by the charges in the PN junction (the so-called built-in field), which is negative (pointing to the left) as expected from the signs of the charges in 3c. Figure 3e is the electric potential (the so-called built-in potential) corresponding to the electric field in Figure 3d. The potential in Figure 3e rises from left to right monotonically. It changes rapidly within the transition zone and is essentially constant far away from there. Since $x_3 = 0$ is chosen as a reference where potential is zero, the potential is negative on the left and positive on the right. The material is piezoelectric. Therefore, the electric field in Figure 3d causes mechanical fields. The displacement field is shown in Figure 3f, which is qualitatively similar to the electric potential. The strain field is shown in Figure 3g, which is localized within and near the transition zone.

Figure 4 shows the effects of $2w$, i.e., the width of the transition zone, on various electromechanical fields. As $2w$ decreases, the transition zone is narrower and all fields change more rapidly there. The total charge in Figure 4c becomes more concentrated. The intensities of the total charge in Figure 4c, the electric field in Figure 4d, and the strain field in Figure 4g all increase. Therefore, in the cases studied in [Luo et al. $\geq$ 2018a; $\geq$ 2018b] where the width of the transition zone $2w = 0$, the intensity or strength of the fields at the PN junction represents that of an ideal or limit case significantly larger than what happens when $2w$ is finite. At far fields away from the transition zone, the concentrations of holes in Figure 4a, electrons in Figure 4b, electric potential in Figure 4e, and displacement in Figure 4f are insensitive to w.

In Figure 5, $w = 0.1\ \mu$m is fixed. The difference of N_D^+ and N_A^- is varied by choosing different values of λ according to

$$a_0 = 10^{21}\ \mathrm{m}^{-3}, \quad a_1 = b_2 = a_0 + \lambda a_0, \quad a_2 = b_1 = 0.8a_0 - \lambda a_0. \tag{51}$$

It can be verified from (36) and (37) that under (51) the sum of N_D^+ and N_A^- is fixed. As λ increases, the gradients of the carrier concentrations increase as seen from Figures 5a and 5b. As a consequence, overall the fields change more rapidly or become stronger inside and near the transition zone, which is as expected.

In Figure 6, $w = 0.1\ \mu$m is fixed. The sum of N_D^+ and N_A^- is varied by choosing different values of λ according to

$$a_0 = 10^{21}\ \mathrm{m}^{-3}, \quad a_1 = b_2 = a_0 + \lambda a_0, \quad a_2 = b_1 = 0.8a_0 + \lambda a_0. \tag{52}$$

It can be verified from (38) that under (52) the difference of N_D^+ and N_A^- is fixed. As λ increases, a_1, a_2, b_1, and b_2 all increase. From (48), p_0 and n_0 increase and hence there are more holes and electrons.

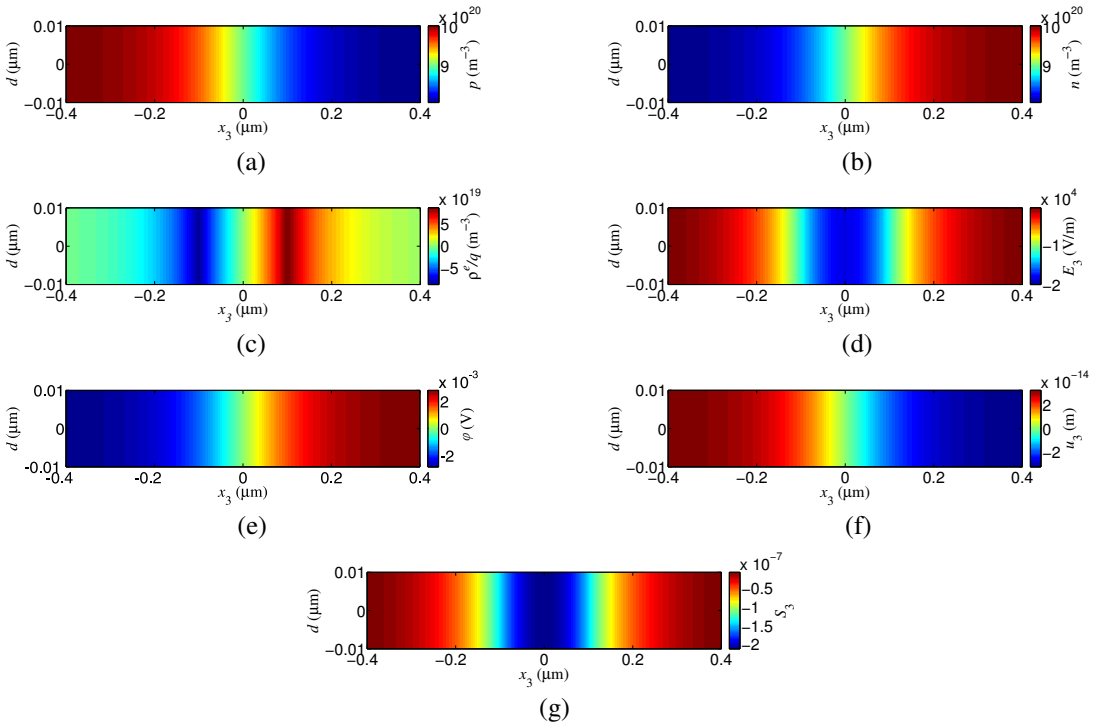

Figure 3. Fields inside and near the transition zone: (a) $p(x_3)$ for holes; (b) $n(x_3)$ for electrons; (c) ρ^e/q for the total charge (PN junction); (d) $E_3(x_3)$ for the electric field; (e) $\varphi(x_3)$ for the electric potential; (f) $u_3(x_3)$ for the displacement; (g) $S_3(x_3)$ for the strain.

This can be seen in Figures 6a and 6b. It can be shown that the coefficients of various fields, C_1, C_3, C_5, and C_6, are inversely proportional to κ^3. This contributes to the reduction of fields in Figure 6c–d as λ, and hence $p_0 + n_0$ as well as κ, increase.

For a qualitative comparison, the results of the PN junction charge and electric field distributions in [Pierret 1996] are shown in Figures 7, left, and 7, right, respectively. Comparing Figures 3c, 4c, 5c and 6c with Figure 7, left, we can see that the piecewise constant charge distribution in Figure 7, left, can be viewed as averages of the gradually changing charge distributions obtained in the present paper, which are more realistic. In obtaining the results in Figure 7, the charge distribution is assumed known so that only the charge equation of electrostatics is needed to calculate the electric field. However, in the present paper coupled equations need to be solved to obtain all fields simultaneously. There is a more fundamental difference between the results obtained in the present paper and that in Figure 7, left. In the assumed charge distribution in Figure 7, left, the impurity N_A^- left by holes alone is responsible for the net charge to the left of the junction and hence the name "depletion region". However, our more sophisticated and coupled-field analysis shows that in fact both the N_A^- left by the holes and the electrons diffused from the right part of the junction together contribute to the net charge to the left of the junction. The situation to the right of the junction is similar. Comparing Figures 3d, 4d, 5d and 6d with Figure 7, right, we see that the axial electric field obtained in the present paper is smoothly changing and hence

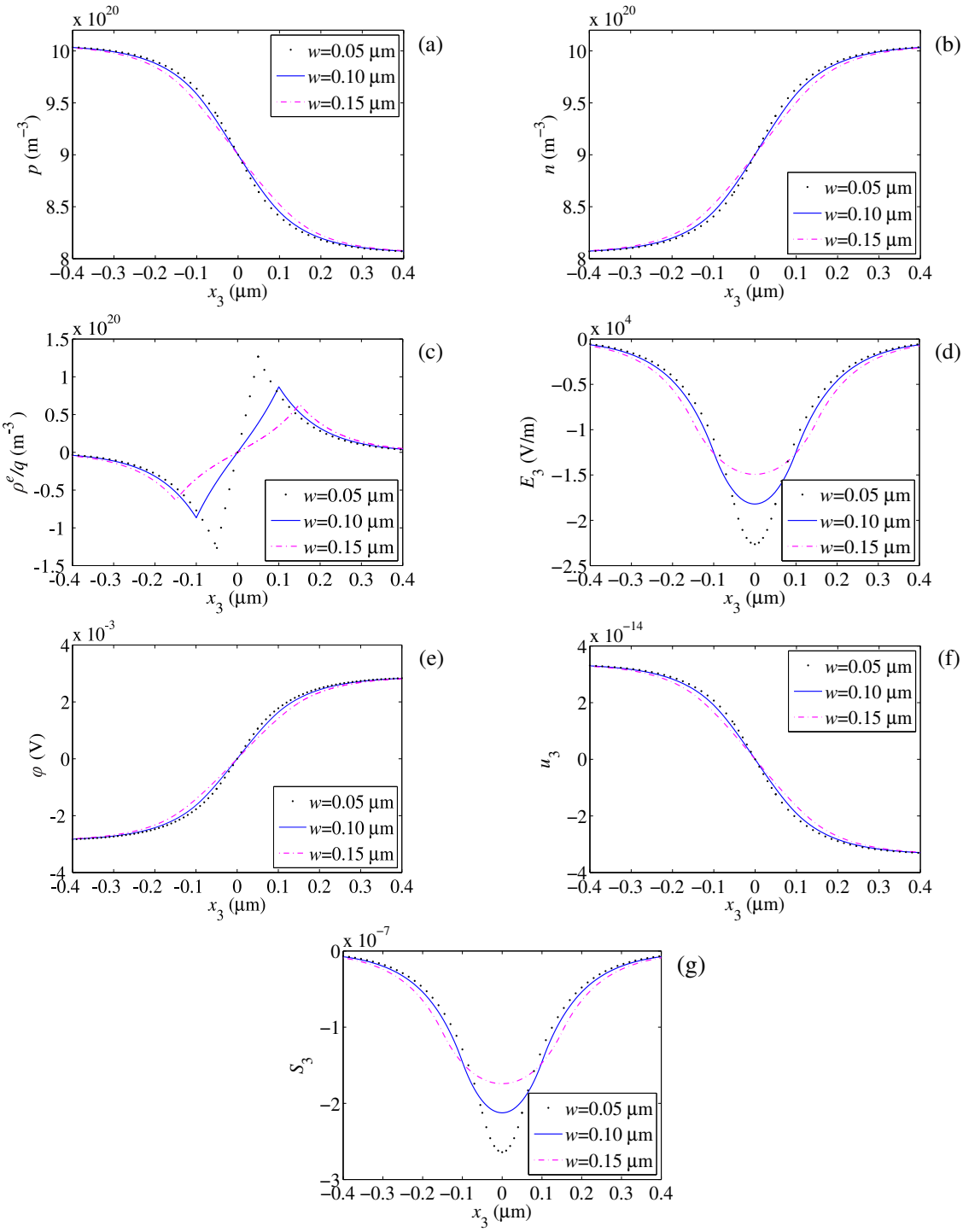

Figure 4. Effects of $2w$, the width of the transition zone: (a) $p(x_3)$ for holes; (b) $n(x_3)$ for electrons; (c) ρ^e/q for the total charge (PN junction); (d) $E_3(x_3)$ for the electric field; (e) $\varphi(x_3)$ for the electric potential; (f) $u_3(x_3)$ for the displacement; (g) $S_3(x_3)$ for the strain.

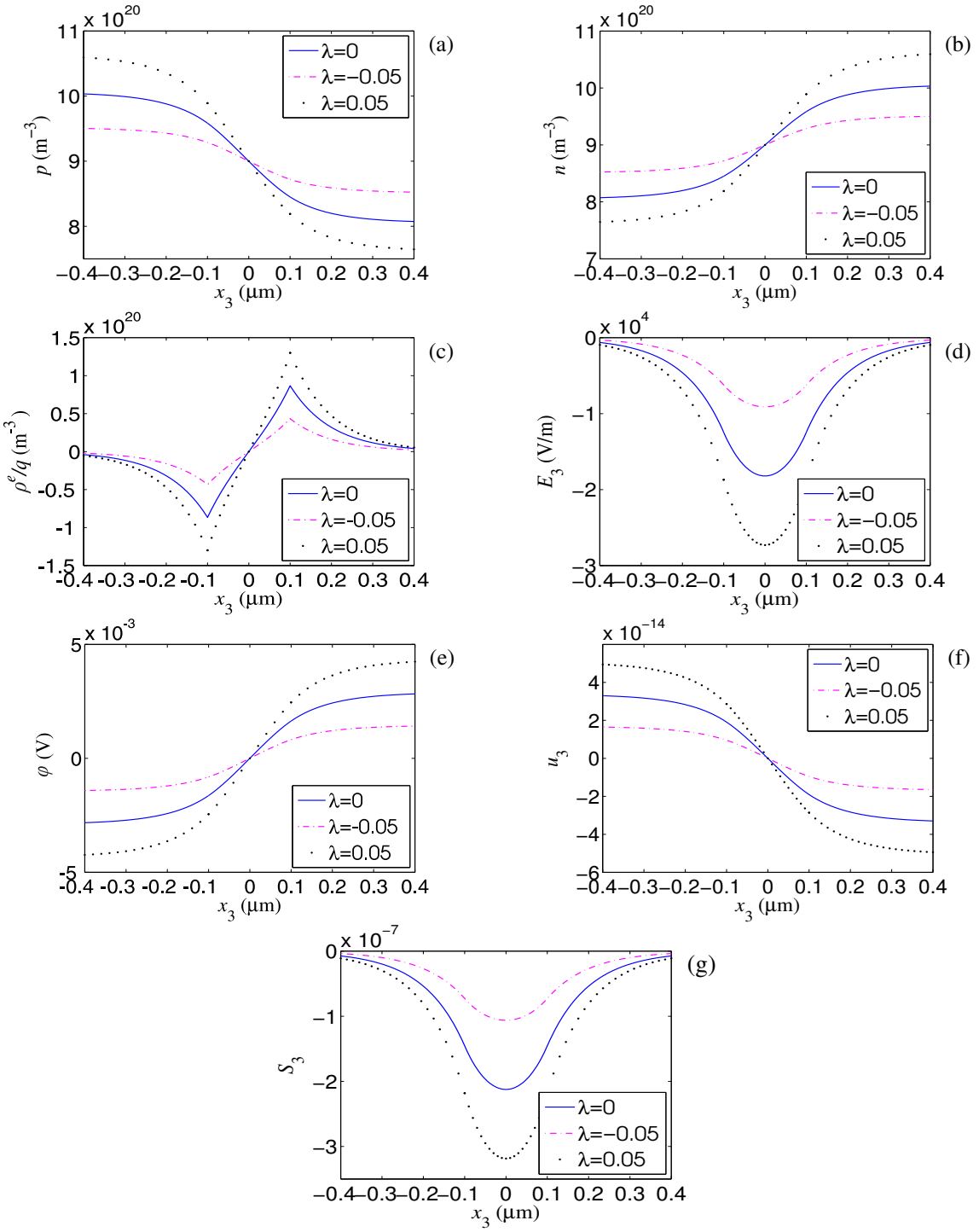

Figure 5. Effects of doping concentration difference: (a) $p(x_3)$ for holes; (b) $n(x_3)$ for electrons; (c) ρ^e/q for the total charge (PN junction); (d) $E_3(x_3)$ for the electric field; (e) $\varphi(x_3)$ for the electric potential; (f) $u_3(x_3)$ for the displacement; (g) $S_3(x_3)$ for the strain.

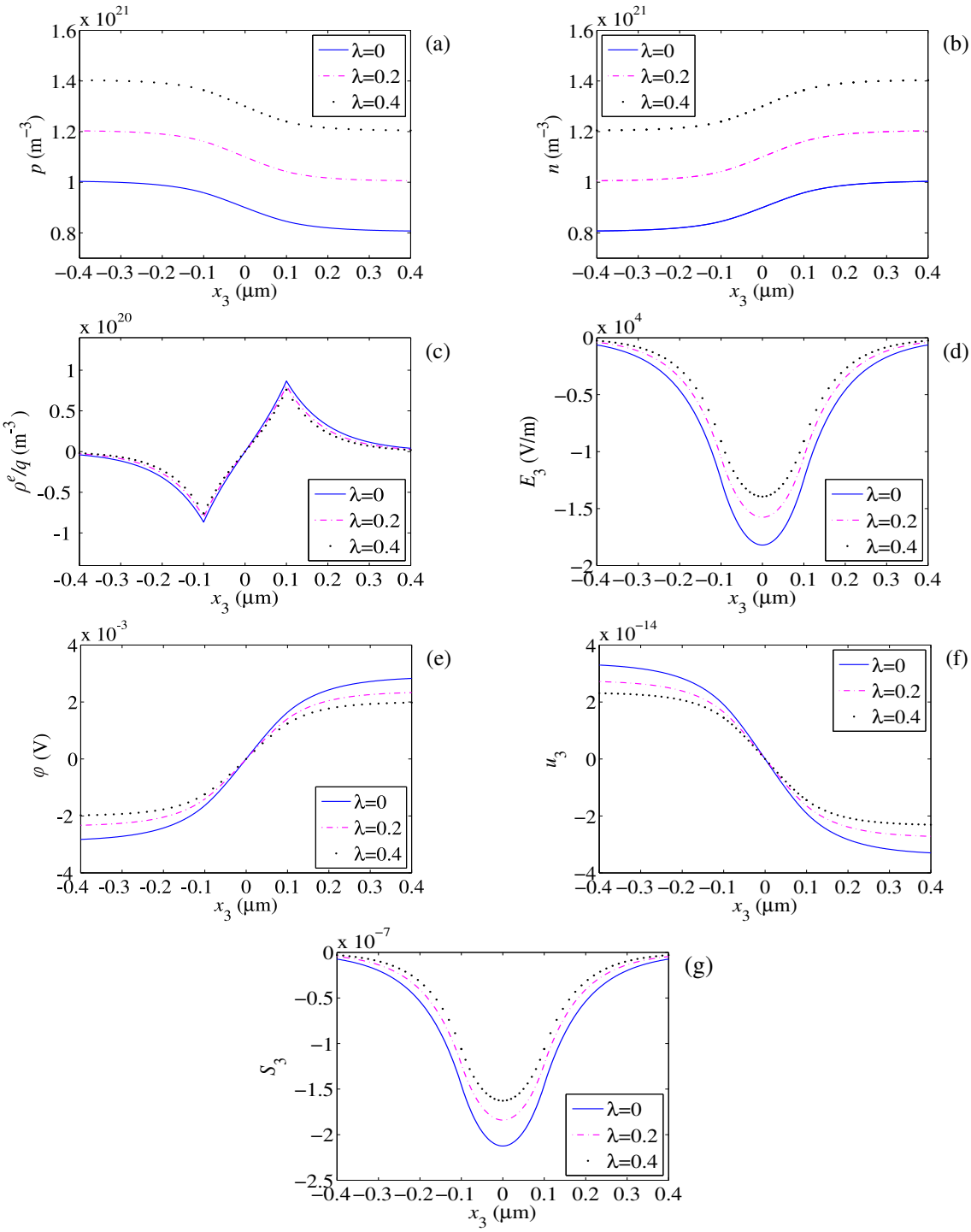

Figure 6. Effects of doping concentration difference: (a) $p(x_3)$ for holes; (b) $n(x_3)$ for electrons; (c) ρ^e/q for the total charge (PN junction); (d) $E_3(x_3)$ for the electric field; (e) $\varphi(x_3)$ for the electric potential; (f) $u_3(x_3)$ for the displacement; (g) $S_3(x_3)$ for the strain.

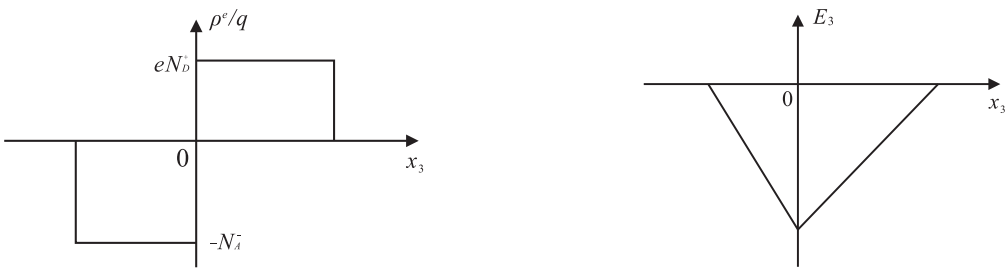

Figure 7. Fields in a PN junction with assumed charge distribution. Left: charge distribution. Right: electric field.

is more realistic. The potential fields obtained in the present paper are qualitatively similar to those in [Pierret 1996], which are not presented here.

7. Sinusoidal doping

In this section we consider the effect of a periodically varying doping described by

$$N_A^-(x_3) = a_1 + b_1 \sin \lambda x_3, \quad N_D^+(x_3) = a_2 + b_2 \sin \lambda x_3. \tag{53}$$

Hence,

$$N_D^+(x_3) - N_A^-(x_3) = a + b \sin \lambda x_3, \quad a = a_2 - a_1, \quad b = b_2 - b_1. \tag{54}$$

In this case, for the particular solution of (21) we have

$$\varphi^p = \frac{q}{\varepsilon_{33}} \left[\frac{a}{\kappa^2} + \frac{b}{\kappa^2 + \lambda^2} \sin \lambda x_3 \right]. \tag{55}$$

From (27) and (28), the two equations for determining p_0 and n_0 take the following form:

$$p_0 - n_0 + a = 0, \quad p_0 = \frac{n_0 a_1}{2n_0 - a_2}. \tag{56}$$

In the special case when $a_2 = a_1$, (54) implies that $a = 0$. Then, from (56), we obtain $p_0 = n_0 = a_1$. For a numerical example, we consider the case when $a_1 = 10^{21}\ \mathrm{m}^{-3}$, $b_1 = 0.2a_1$, $b_2 = -b_1$, and $\lambda = 0.2\kappa$. Then $2\pi/\lambda \cong 3\mu$m, which can be viewed as some wavelength of the doping. We choose $2L = 30\ \mu$m which is about ten times the doping wavelength $2\pi/\lambda$. The electromechanical fields in this case are shown in Figure 8. They are essentially periodic except at $x_3 = \pm L$ where there are some end effects. It can be seen that under a periodic doping, p and n in Figure 8a vary similarly but are out of phase. The total charge ρ^e in Figure 8b oscillates and has some concentration near the ends. The concentration of carriers near the ends of a rod was also observed in [Zhang et al. 2016a; 2017a]. The periodic doping produces essentially the same periodic electric field in Figure 8c, potential in Figure 8d, displacement in Figure 8e, and strain in Figure 8f. Effectively a periodic doping produces a series of PN junctions. The fields in Figure 8 can be explored for possible applications. For example, if an acoustic wave propagates in the rod with the presence of the periodic strain field in Figure 8f, does the strain field acts as an initial or biasing field and does it affect the waves like a phononic crystal?

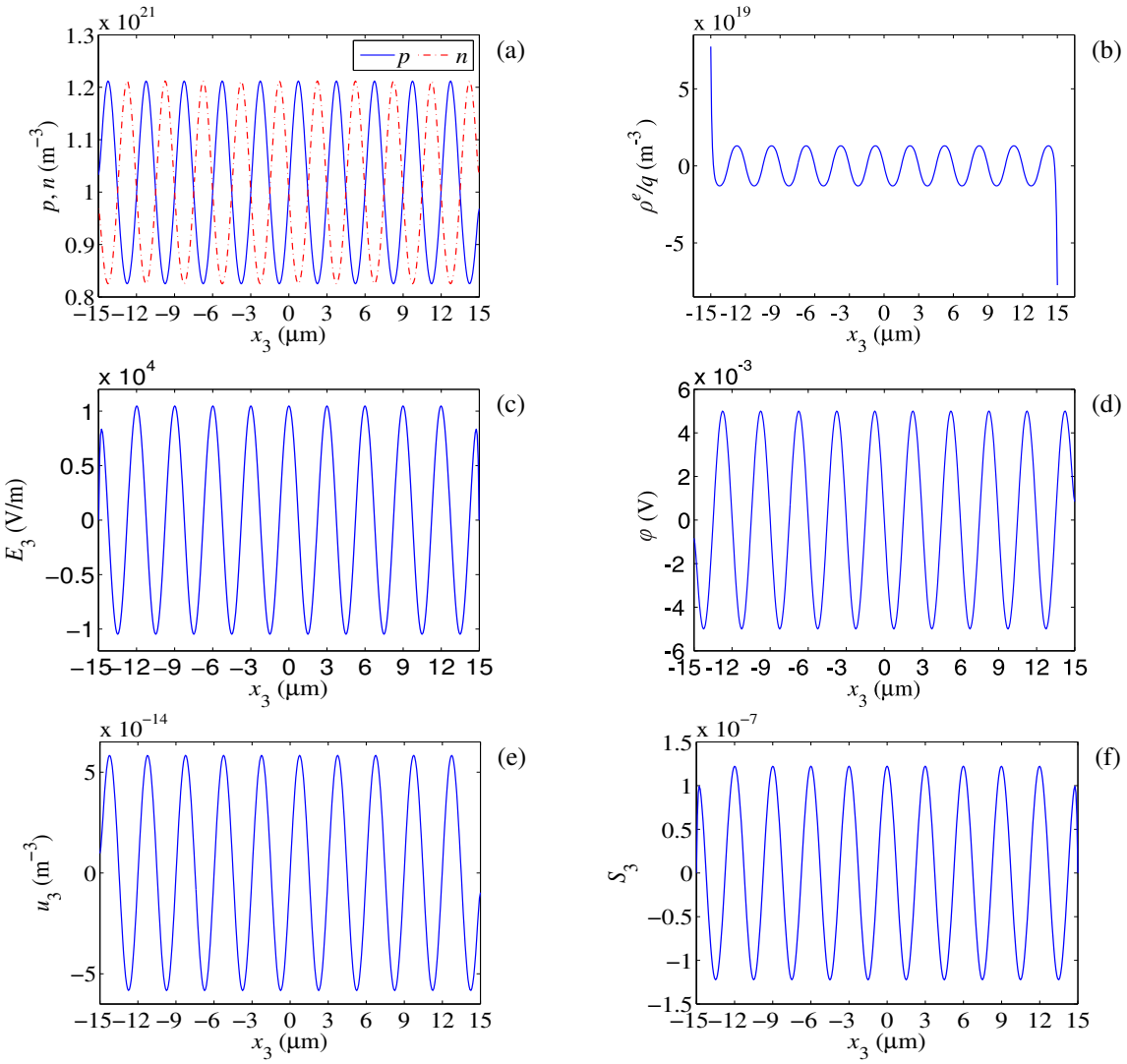

Figure 8. Effects of sinusoidal doping: (a) $p(x_3)$ and $n(x_3)$; (b) ρ^e/q for the total charge; (c) $E_3(x_3)$ for the electric field; (d) $\varphi(x_3)$ for the electric potential; (e) $u_3(x_3)$ for the displacement; (f) $S_3(x_3)$ for the strain.

8. Conclusions

For low values of the electric potential, the governing equations of an isolated piezoelectric semiconductor rod can be linearized and reduced to a single equation for the potential which is valid for small carrier concentration variations. Solutions of the equation show that a uniform or linear doping makes a uniform or linear contribution to the electric potential and carrier concentrations. PN junctions can be realized through nonuniform doping. Near the transition zone between a p-doped region and an n-doped region, there are local charges producing a local electric field and thus forming a PN junction. In the

so-called depletion regions near a PN junction, in fact both impurities and mobile charges contribute to the net charges. The intensity or strength of the charge and field distributions at the junction is sensitive to the width of the transition zone of the piecewise linear doping. When its width becomes narrower, the electric field in the PN junction becomes stronger. The electric field in the junction also becomes stronger when the doping difference increases. A sinusoidal doping produces periodic distributions of charges and an electric field which can be explored for device applications. Since the material is piezoelectric, there exist mechanical fields associated with the electric fields.

Acknowledgments

This work was supported by the National Natural Science Foundation of China (Nos. 11672141 and 11372145), the Y. K. Pao Visiting Professorship at Ningbo University, and the K. C. Wong Magana Fund through Ningbo University.

References

[Araneo et al. 2012] R. Araneo, G. Lovat, P. Burghignoli, and C. Falconi, "Piezo-semiconductive quasi-1D nanodevices with or without anti-symmetry", *Adv. Mater.* **24**:34 (2012), 4719–4724.

[Asthana et al. 2014] A. Asthana, H. A. Ardakani, Y. K. Yap, and R. S. Yassar, "Real time observation of mechanically triggered piezoelectric current in individual ZnO nanobelts", *J. Mater. Chem. C* **2**:20 (2014), 3995–4004.

[Auld 1973] B. A. Auld, *Acoustic fields and waves in solids, I*, Wiley, New York, 1973.

[Büyükköse et al. 2014] S. Büyükköse, A. Hernández-Mínguez, B. Vratzov, C. Somaschini, L. Geelhaar, H. Riechert, W. G. van der Wiel, and P. V. Santos, "High-frequency acoustic charge transport in GaAs nanowires", *Nanotechnology* **25**:13 (2014), art. id. 135204.

[Chen et al. 2007] T. T. Chen, C. L. Cheng, S.-P. Fu, and Y. F. Chen, "Photoelastic effect in ZnO nanorods", *Nanotechnology* **18**:22 (2007), art. id. 225705.

[Choi et al. 2009] M.-Y. Choi, D. Choi, M.-J. Jin, I. Kim, S.-H. Kim, J.-Y. Choi, S. Y. Lee, J. M. Kim, and S.-W. Kim, "Mechanically powered transparent flexible charge-generating nanodevices with piezoelectric ZnO nanorods", *Adv. Mater.* **21**:21 (2009), 2185–2189.

[Chung et al. 2012] S. Y. Chung, S. Kim, J.-H. Lee, K. Kim, S.-W. Kim, C.-Y. Kang, S.-J. Yoon, and Y. S. Kim, "All-solution-processed flexible thin film piezoelectric nanogenerator", *Adv. Mater.* **24**:45 (2012), 6022–6027.

[Collet 2008] B. Collet, "Acoustic wave propagation in cubic piezoelectric semiconductor plates", *J. Acoust. Soc. Am.* **123**:5 (2008), 3694.

[Fan et al. 2016] C. Y. Fan, Y. Yan, G. T. Xu, and M. H. Zhao, "Piezoelectric-conductor iterative method for analysis of cracks in piezoelectric semiconductors via the finite element method", *Eng. Fract. Mech.* **165** (2016), 183–196.

[Fan et al. 2017] S. Fan, Y. Liang, J. Xie, and Y. Hu, "Exact solutions to the electromechanical quantities inside a statically-bent circular ZnO nanowire by taking into account both the piezoelectric property and the semiconducting performance, I: linearized analysis", *Nano Energy* **40** (2017), 82–87.

[Gao and Wang 2007] Y. Gao and Z. L. Wang, "Electrostatic potential in a bent piezoelectric nanowire: the fundamental theory of nanogenerator and nanopiezotronics", *Nano Lett.* **7**:8 (2007), 2499–2505.

[Gao and Wang 2009] Y. Gao and Z. L. Wang, "Equilibrium potential of free charge carriers in a bent piezoelectric semiconductive nanowire", *Nano Lett.* **9**:3 (2009), 1103–1110.

[Gao et al. 2007] P. X. Gao, J. Song, J. Liu, and Z. L. Wang, "Nanowire piezoelectric nanogenerators on plastic substrates as flexible power sources for nanodevices", *Adv. Mater.* **19**:1 (2007), 67–72.

[Gu and Jin 2015] C. Gu and F. Jin, "Shear-horizontal surface waves in a half-space of piezoelectric semiconductors", *Philos. Mag. Lett.* **95**:2 (2015), 92–100.

[Hickernell 2003] F. S. Hickernell, "The piezoelectric semiconductor and acoustoelectronic device development in the sixties", pp. 1012–1020 in *Proc. 2003 IEEE International Frequency Control Symposium and PDA Exhibition* (Tampa), IEEE, Piscataway, NJ, 2003.

[Hu et al. 2007] Y. Hu, Y. Zeng, and J. Yang, "A mode III crack in a piezoelectric semiconductor of crystals with 6 mm symmetry", *Int. J. Solids Struct.* **44**:11-12 (2007), 3928–3938.

[Hu et al. 2010] Y. Hu, Y. Chang, P. Fei, R. L. Snyder, and Z. L. Wang, "Designing the electric transport characteristics of ZnO micro/nanowire devices by coupling piezoelectric and photoexcitation effects", *ACS Nano* **4**:2 (2010), 1234–1240.

[Hutson and White 1962] A. R. Hutson and D. L. White, "Elastic wave propagation in piezoelectric semiconductors", *J. Appl. Phys.* **33**:40 (1962), 40–47.

[Ji et al. 2013] J. Ji, Z. Zhou, X. Yang, W. Zhang, S. Sang, and P. Li, "One-dimensional nano-interconnection formation", *Small* **9**:18 (2013), 3014–3029.

[Kumar and Kim 2011] B. Kumar and S.-W. Kim, "Recent advances in power generation through piezoelectric nanogenerators", *J. Mater. Chem.* **21**:47 (2011), 18946–18958.

[Lee et al. 2012] K. Y. Lee, B. Kumar, J.-S. Seo, K.-H. Kim, J. I. Sohn, S. N. Cha, D. Choi, Z. L. Wang, and S.-W. Kim, "P-type polymer-hybridized high-performance piezoelectric nanogenerators", *Nano Lett.* **12**:4 (2012), 1959–1964.

[Lee et al. 2014] K. Y. Lee, J. Bae, S. M. Kim, J.-H. Lee, G. C. Yoon, M. K. Gupta, S. Kim, H. Kim, J. Park, and S.-W. Kim, "Depletion width engineering via surface modification for high performance semiconducting piezoelectric nanogenerators", *Nano Energy* **8** (2014), 165–173.

[Li et al. 2015] P. Li, F. Jin, and J. Yang, "Effects of semiconduction on electromechanical energy conversion in piezoelectrics", *Smart Mater. Struct.* **24** (2015), art. id. 025021.

[Li et al. $\geq$ 2018] P. Li, F. Jin, and J. X. Ma, "The one-dimensional dynamic equations for piezoelectric semiconductor beams with rectangular cross sections and its applications in static and dynamic characteristics analysis", to appear in *Appl. Math. Mech.*

[Liao et al. 2014] Q. Liao, Z. Zhang, X. Zhang, M. Mohr, Y. Zhang, and H.-J. Fecht, "Flexible piezoelectric nanogenerators based on a fiber/ZnO nanowires/paper hybrid structure for energy harvesting", *Nano Res.* **7**:6 (2014), 917–928.

[Luo et al. $\geq$ 2018a] Y. X. Luo, C. L. Zhang, W. Q. Chen, and J. S. Yang, "An analysis of PN junctions in piezoelectric semiconductors", to appear in *J. Appl. Phys.*

[Luo et al. $\geq$ 2018b] Y. X. Luo, C. L. Zhang, W. Q. Chen, and J. S. Yang, "Electromechanical fields near a circular PN junction between two piezoelectric semiconductors", to appear in *Acta Mech. Solida Sin.*

[Pierret 1983] R. F. Pierret, *Semiconductor fundamentals*, Modular Series on Solid State Devices **1**, Addison-Wesley, Reading, MA, 1983.

[Pierret 1996] R. F. Pierret, *Semiconductor device fundamentals*, Addison-Wesley, Reading, MA, 1996.

[Romano et al. 2011] G. Romano, G. Mantini, A. Di Carlo, A. D'Amico, C. Falconi, and Z. L. Wang, "Piezoelectric potential in vertically aligned nanowires for high output nanogenerators", *Nanotechnology* **22**:46 (2011), art. id. 465401.

[Shen et al. 2010] Y. Shen, J.-I. Hong, S. Xu, S. Lin, H. Fang, S. Zhang, Y. Ding, R. L. Snyder, and Z. L. Wang, "A general approach for fabricating arc-shaped composite nanowire arrays by pulsed laser deposition", *Adv. Funct. Mater.* **20**:5 (2010), 703–707.

[Sladek et al. 2014a] J. Sladek, V. Sladek, E. Pan, and M. Wünsche, "Fracture analysis in piezoelectric semiconductors under a thermal load", *Eng. Fract. Mech.* **126** (2014), 27–39.

[Sladek et al. 2014b] J. Sladek, V. Sladek, E. Pan, and D. L. Young, "Dynamic anti-plane crack analysis in functional graded piezoelectric semiconductor crystals", *Comput. Model. Eng. Sci.* **99**:4 (2014), 273–296.

[Wang 2003] Z. L. Wang, "Nanobelts, nanowires, and nanodiskettes of semiconducting oxides: from materials to nanodevices", *Adv. Mater.* **15**:5 (2003), 432–436.

[Wang 2010] Z. L. Wang, "Piezopotential gated nanowire devices: piezotronics and piezo-phototronics", *Nano Today* **5**:6 (2010), 540–552.

[Wang et al. 2006] X. Wang, J. Zhou, J. Song, J. Liu, N. Xu, and Z. L. Wang, "Piezoelectric field effect transistor and nanoforce sensor based on a single ZnO nanowire", *Nano Lett.* **6**:12 (2006), 2768–2772.

[Wauer and Suherman 1997] J. Wauer and S. Suherman, "Thickness vibrations of a piezo-semiconducting plate layer", *Int. J. Eng. Sci.* **35**:15 (1997), 1387–1404.

[Xue et al. 2010] H. Xue, N. Pan, M. Li, Y. Wu, X. Wang, and J. G. Hou, "Probing the strain effect on near band edge emission of a curved ZnO nanowire via spatially resolved cathodoluminescence", *Nanotechnology* **21**:21 (2010), art. id. 215701.

[Yang 2005] J. Yang, "An anti-plane crack in a piezoelectric semiconductor", *Int. J. Fract.* **136**:1-4 (2005), L27–L32.

[Yang and Zhou 2005] J. S. Yang and H. G. Zhou, "Amplification of acoustic waves in piezoelectric semiconductor plates", *Int. J. Solids Struct.* **42**:11-12 (2005), 3171–3183.

[Yang et al. 2005] J. Yang, X. Yang, and J. A. Turner, "Amplification of acoustic waves in piezoelectric semiconductor shells", *J. Intell. Mater. Syst. Struct.* **16**:7-8 (2005), 613–621.

[Yang et al. 2006] J. S. Yang, Y. C. Song, and A. K. Soh, "Analysis of a circular piezoelectric semiconductor embedded in a piezoelectric semiconductor substrate", *Arch. Appl. Mech.* **76**:7-8 (2006), 381–390.

[Yoo et al. 2009] J. Yoo, C.-H. Lee, Y.-J. Doh, H. S. Jung, and G.-C. Yi, "Modulation doping in ZnO nanorods for electrical nanodevice applications", *Appl. Phys. Lett.* **94**:22 (2009), art. id. 223117.

[Yu et al. 2010] J. Yu, S. J. Ippolito, W. Wlodarski, M. Strano, and K. Kalantar-Zadeh, "Nanorod based Schottky contact gas sensors in reversed bias condition", *Nanotechnology* **21**:26 (2010), art. id. 265502.

[Zhang and Hu 2014] J. Zhang and Y.-T. Hu, "Analysis on the anti-plane deformations of a piezoelectric semiconductor plate with a hole", pp. 106–109 in *Proc. 2014 Symposium on Piezoelectricity, Acoustic Waves, and Device Applications* (Beijing), edited by X. Wang et al., IEEE, Piscataway, NJ, 2014.

[Zhang et al. 2016a] C. L. Zhang, X. Y. Wang, W. Q. Chen, and J. S. Yang, "Carrier distribution and electromechanical fields in a free piezoelectric semiconductor rod", *J. Zhejiang Univ. Sci. A* **17**:1 (2016), 37–44.

[Zhang et al. 2016b] C. L. Zhang, X. Y. Wang, W. Q. Chen, and J. S. Yang, "Propagation of extensional waves in a piezoelectric semiconductor rod", *AIP Adv.* **6**:4 (2016), art. id. 045301.

[Zhang et al. 2017a] C. Zhang, X. Wang, W. Chen, and J. Yang, "An analysis of the extension of a ZnO piezoelectric semiconductor nanofiber under an axial force", *Smart Mater. Struct.* **26**:2 (2017), art. id. 025030.

[Zhang et al. 2017b] C. L. Zhang, Y. X. Luo, R. R. Cheng, and X. Y. Wang, "Electromechanical fields in piezoelectric semiconductor nanofibers under an axial force", *Mater. Res. Soc. Adv.* **2**:56 (2017), 3421–3426.

[Zhang et al. $\geq$ 2018] C. L. Zhang, X. Y. Wang, W. Q. Chen, and J. S. Yang, "Bending of a cantilever piezoelectric semiconductor fiber under an end force", under review.

[Zhao et al. 2016a] M. H. Zhao, Y. Li, Y. Yan, and C. Y. Fan, "Singularity analysis of planar cracks in three-dimensional piezoelectric semiconductors via extended displacement discontinuity boundary integral equation method", *Eng. Anal. Bound. Elem.* **67** (2016), 115–125.

[Zhao et al. 2016b] M. H. Zhao, Y. B. Pan, C. Y. Fan, and G. T. Xu, "Extended displacement discontinuity method for analysis of cracks in 2D piezoelectric semiconductors", *Int. J. Solids Struct.* **94** (2016), 50–59.

Received 2 Sep 2017. Revised 24 Sep 2017. Accepted 29 Sep 2017.

GUANGYING YANG: 1501081004@nbu.edu.cn
Mechanical Engineering and Mechanics, Ningbo University, Ningbo, China

JIANKE DU: dujianke@nbu.edu.cn
Mechanical Engineering and Mechanics, Ningbo University, Ningbo, China

JI WANG: wangji@nbu.edu.cn
Mechanical Engineering and Mechanics, Ningbo University, Ningbo, China

JIASHI YANG: jyang1@unl.edu
Mechanical and Materials Engineering, University of Nebraska – Lincoln, NE, United States